Resonance fluorescence and phase-dependent spectra of a singly charged *n*-doped quantum dot in the Voigt geometry

F. Carreño,[1] S. Maede-Razavi,[2] and M. A. Antón[1]
[1]*Facultad de Óptica y Optometría, Universidad Complutense de Madrid, Calle Arcos de Jalón 118, 28037 Madrid, Spain*
[2]*Department of Physics, College of Science, University of Yasouj, Yasouj, Iran*
(Received 3 October 2016; revised manuscript received 29 March 2017; published 19 May 2017)

We report on the resonance fluorescence and phase-dependent spectra in singly charged *n*-doped quantum dots in the presence of a strong external magnetic field in the Voigt geometry. The use of a nonresonant laser field driving two of the four active transitions results in the obtention of fluorescent photons along the four channels. The fluorescent photons coming from the two undriven transitions exhibit sidebands whose spectral location can be tuned through the Rabi frequency of the driving field and, most interestingly, their linewidths remain subnatural even for large values of the Rabi frequency of the laser field. It is shown that those sidebands present quantum fluctuations below the fundamental limit set by vacuum fluctuations. The numerical findings are fully explained by considering how the dressed states evolve in terms of the external physical magnitudes: the detuning, the Rabi frequency, and the dephasing rates.

DOI: 10.1103/PhysRevB.95.195310

I. INTRODUCTION

Semiconductor quantum dots (QDs) are analogous to real atoms, and their optical properties closely resemble the ones found in atomic physics. Many quantum optical effects—such as the coherent manipulation of exciton wave functions [1], optical pumping [2–6], resonance fluorescence [7–23], rotations of the spin vector [24–28], coherent population trapping [29–32], single photon generation [16,20,33,34]—are the subjects of stimulating experiments which have revealed their potential in quantum information science.

The possibility of realizing a spin-photon interface has been stimulated by the demonstration that the scattered photons by a solid-state emitter are correlated with the quantum dot spin [9,14]. One key element of a quantum repeater protocol is the creation of entanglement between two distant quantum emitters by overlapping spectrally identical single photons [11]. However, the spectral inhomogeneity of these emitters poses a significant challenge. An important aspect in terms of quantum information processing is the tunability of the resonantly scattered photons. In order to accomplish this task, an independent knob to ensure the spectral overlap of the emitted photons is needed.

The experimental observation of all-optical tunable Raman photons [11] was a first step towards the probabilistic entanglement of two distant *p*-doped QDs in the Voigt geometry [35]. The Raman photons were produced in an optically driven quantum dot characterized as a Λ three-level system. It was shown that by detuning the driving laser from resonance, the frequency of the Raman photons could be tuned either by changing this external detuning or the lower level's splitting by changing the magnitude of the external magnetic field. However, in single self-assembled QDs charged with a single excess conduction-band electron and subject to a high magnetic field in the Voigt geometry, a four-level description could provide a more accurate description of the system up to a field strength of a few teslas. In this case both ground states are optically coupled to the trion states. The four-level model has been previously considered to analyze the fidelity of spin-state preparation [4].

The aim of this work is to extend previous investigations [11] of the spectral properties of fluorescent Raman photons scattered by a gated *n*-doped QD in the Voigt geometry which is driven by an out-of-resonance laser field, taking into account the fact that the driving field couples the ground states to the trion states. We make use of a master equation for the density matrix equation for the four-level system of a X^{1-} in a magnetic field. Our treatment generalizes the usual analysis which reduces the system to a three-level type as in Refs. [8,11,21]. We show that even if the driven field populates the trion states, the strength of the driving field can be used as an additional knob to tune the center frequency of the Raman photons, keeping subnatural the linewidth of the corresponding spectral line. In addition, we analyze within the four-level scheme the phase-dependent spectrum of the scattered photons. It is found that the subnatural Raman lines exhibit a level of squeezing below the limit set by vacuum fluctuations. We also show how these phenomena can be explained by moving to the dressed state picture. It is worth mentioning that in a recent experiment, Schulte *et al.* have shown that by using a QD with a large optical dipole moment, and modeling it as a two-level system, quadrature squeezing and antibunching have been obtained simultaneously [36]. The noise spectrum of a QD in close proximity to a graphene sheet has been analyzed also, showing that surface plasmons strongly influence the level of squeezing of the scattered radiation [37].

The paper is organized as follows: Sec. II establishes the model, i.e., the Hamiltonian of the system and the time-evolution equations of the atomic operators assuming the rotating-wave approximation. Section III present the results of numerical simulations together with a physical explanation of the different effects found. Finally, Sec. IV summarizes the main conclusions.

II. THEORETICAL MODEL

We consider InAs/GaAs self-assembled QDs via the Stranski-Krastanov method with growth direction along the

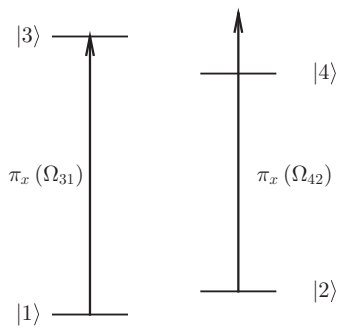

FIG. 1. Four-level system including the relevant transitions when the external magnetic field is applied perpendicular to the growth direction. Transitions $|1\rangle \leftrightarrow |3\rangle$ and $|2\rangle \leftrightarrow |4\rangle$ are driven by a π_x polarized laser field (Ω_3), while transitions $|1\rangle \leftrightarrow |4\rangle$ and $|2\rangle \leftrightarrow |3\rangle$ could be driven by a π_y laser field (not shown).

Z axis. The QDs are separated from a Fermi sea of electrons by several nanometers in thick n-doped back contact layer. An external bias voltage applied between the top gate and the back contact allows the deterministic charge of the QD [38,39]. The ground spin states are labeled $|1_z\rangle \equiv |\downarrow_z\rangle$ and $|2_z\rangle \equiv |\uparrow_z\rangle$, while the excited trion states are $|4_z\rangle \equiv |\downarrow_z \uparrow_z \Downarrow_z\rangle$ and $|3_z\rangle \equiv |\downarrow_z \uparrow_z \uparrow_z\rangle$. Here $\uparrow_z(\downarrow_z)$ and $\uparrow_z(\downarrow_z)$ denote a heavy hole and an electron with spins along (against) the Z axis. Electron and trion states share the same energy level in the absence of an external magnetic field. The energy level diagram of such kind of QD is depicted in Fig. 1(a). The optical transition $|1_z\rangle \leftrightarrow |4_z\rangle$ ($|2_z\rangle \leftrightarrow |3_z\rangle$) is driven by a σ^- (σ^+) polarized laser field, while due to selection rules transitions $|1_z\rangle \leftrightarrow |3_z\rangle$ and $|2_z\rangle \leftrightarrow |4_z\rangle$ remain dark. The application of an external magnetic field along the X axis (perpendicular to the Z axis), in the so-called Voigt geometry, lifts the degeneracy of hole/electron levels according to $E_{Zm}^{h(e)} = \frac{1}{2}\mu_B g^{h(e)} B_x$, where $E_{Zm}^{h(e)}$ stands for the Zeeman energy shift relative to $B_x = 0$ T, B_x being the external magnetic field, and μ_B is the Bohr magneton. Quantity $g^{h(e)}$ is the Landé factor of carrier h (e). The external magnetic field also causes a reference frame transformation from the Z axis to the X axis, and we get $|2\rangle \equiv |\uparrow_x\rangle = 1/\sqrt{2}(|\uparrow_z\rangle + |\downarrow_z\rangle)$ and $|1\rangle \equiv |\downarrow_x\rangle = 1/\sqrt{2}(|\uparrow_z\rangle - |\downarrow_z\rangle)$. Now each ground state is linked to the two exciton states ($|4\rangle \equiv |\downarrow_x \uparrow_x \downarrow_x\rangle$ and $|3\rangle \equiv |\downarrow_x \uparrow_x \uparrow_x\rangle$) via linearly and orthogonally polarized transitions, as depicted in Fig. 1(b).

The Hamiltonian that governs the dynamics of the QD can be expressed in the rotating-f approximation as

$$H = H_A + H_{\text{Int}}. \tag{1}$$

The free Hamiltonian H_A of the system reads as

$$H_A = \hbar \sum_{j=1}^{4} \omega_j \sigma_{jj}, \tag{2}$$

where $\hbar\omega_j$ is the energy of the jth level and σ_{ij} are the Pauli operators.

The interaction Hamiltonian H_{Int}, written as

$$H_{\text{Int}} = -\hbar(\Omega_{31} e^{-i\omega_L t}\sigma_{31} + \Omega_{42} e^{-i\omega_L t}\sigma_{42} + \text{H.a.}), \tag{3}$$

accounts for the interaction of the QD with the optical field of angular frequency ω_L which drives transitions $|1\rangle \leftrightarrow |3\rangle$ and $|2\rangle \leftrightarrow |4\rangle$, while transition transitions $|1\rangle \leftrightarrow |4\rangle$ and $|2\rangle \leftrightarrow |3\rangle$ remain undriven. The Rabi frequencies are given by $\Omega_{31} = \vec{\mu}_{13} \cdot \vec{E}_0\hbar/2$ and $\Omega_{42} = \vec{\mu}_{24} \cdot \vec{E}_0\hbar/2$, $\vec{E}_0$ being the slowly varying amplitude of the optical field.

Let us consider the following unitary transformation $U(t) = e^{-i\omega_L(\sigma_{33}+\sigma_{44})t}$. The new Hamiltonian should read as

$$\begin{aligned} H' &= U^\dagger(t)HU(t) - i\hbar U^\dagger(t)\frac{\partial}{\partial t}U(t) \\ &= \hbar\omega_1\sigma_{11} + \hbar\omega_2\sigma_{22} + \hbar(\omega_3 - \omega_L)\sigma_{33} + \hbar(\omega_4 - \omega_L)\sigma_{44} \\ &\quad - \hbar(\Omega_{31}\sigma_{31} + \Omega_{42}\sigma_{42} + \text{H.a.}). \end{aligned} \tag{4}$$

Since we are considering a closed system ($\sum_{j=1}^{4}\sigma_{jj} = \hat{I}$, $\hat{I}$ being the identity operator), Eq. (4) can be rewritten as

$$\begin{aligned} H' &= \hbar\omega_1\hat{I} + \hbar\omega_{21}\sigma_{22} + \hbar(\omega_{31} - \omega_L)\sigma_{33} + \hbar(\omega_{41} - \omega_L)\sigma_{44} \\ &\quad - \hbar(\Omega_{31}\sigma_{31} + \Omega_{42}\sigma_{42} + \text{H.a.}). \end{aligned} \tag{5}$$

Let us define the optical detuning as $\delta \equiv \omega_{31} - \omega_L$, then Eq. (5) can be rewritten as

$$\begin{aligned} H' &= +\hbar\omega_{21}\sigma_{22} + \hbar\delta\sigma_{33} + \hbar(\delta - \omega_{34})\sigma_{44} \\ &\quad - \hbar(\Omega_{31}\sigma_{31} + \Omega_{42}\sigma_{42} + \text{H.a.}), \end{aligned} \tag{6}$$

where the constant term $\hbar\omega_1\hat{I}$ has been dropped.

The dissipation processes are described through operator $\mathcal{L}\rho$, which in the Linblad form reads as

$$\begin{aligned} \mathcal{L}\rho &= \Gamma_{12}\sigma_{21}\rho\sigma_{12} - \frac{\Gamma_{12}}{2}(\sigma_{11}\rho + \rho\sigma_{11}) \\ &\quad + \Gamma_{21}\sigma_{12}\rho\sigma_{21} - \frac{\Gamma_{21}}{2}(\sigma_{22}\rho + \rho\sigma_{22}) \\ &\quad + \Gamma_{31}\sigma_{13}\rho\sigma_{31} - \frac{\Gamma_0}{2}(\sigma_{33}\rho + \rho\sigma_{33}) \\ &\quad + \Gamma_{41}\sigma_{14}\rho\sigma_{41} - \frac{\Gamma_0}{2}(\sigma_{44}\rho + \rho\sigma_{44}) \\ &\quad + \Gamma_{32}\sigma_{23}\rho\sigma_{32} - \frac{\Gamma_0}{2}(\sigma_{33}\rho + \rho\sigma_{33}) \\ &\quad + \Gamma_{42}\sigma_{24}\rho\sigma_{42} - \frac{\Gamma_0}{2}(\sigma_{44}\rho + \rho\sigma_{44}) \\ &\quad + \gamma_{22}\sigma_{22}\rho\sigma_{22} - \frac{\gamma_{22}}{2}(\sigma_{22}\rho + \rho\sigma_{22}) \\ &\quad + \gamma_{11}\sigma_{11}\rho\sigma_{11} - \frac{\gamma_{11}}{2}(\sigma_{11}\rho + \rho\sigma_{11}). \end{aligned} \tag{7}$$

The terms involving Γ_{kj} arise from Linblad operators $L(\sqrt{\Gamma_{kj}}\sigma_{jk})$ ($j = 1,2, k = 3,4$) and they account for the spontaneous photons produced along transitions $|k\rangle \leftrightarrow |j\rangle$. The action of a Linblad operator is defined as $L(C) = C\rho C^\dagger - \frac{1}{2}(\rho C^\dagger C + C^\dagger C\rho)$. The term proportional to γ_{ii} ($i = 1,2$) accounts for pure dephasing whereas the terms proportional to Γ_{21}, and Γ_{12} arise from an incoherent relaxation process which couples states $|1\rangle \leftrightarrow |2\rangle$ bidirectionally. They arise from exchange interaction with the Fermi sea of electrons in the back contact giving rise to spin-flip cotunneling.

The density matrix equations of motion of the system read as

$$\begin{aligned}
\frac{\partial\rho_{22}}{\partial t} &= -(\Gamma_{21}+\Gamma_{12})\rho_{22}+(\Gamma_{32}-\Gamma_{12})\rho_{33}+(\Gamma_{42}-\Gamma_{12})\rho_{44}\\
&\quad -i\Omega_{42}\rho_{24}+i\Omega_{42}^{*}\rho_{42},\\
\frac{\partial\rho_{33}}{\partial t} &= -(\Gamma_{32}+\Gamma_{31})\rho_{33}+i\Omega_{31}\rho_{13}-i\Omega_{31}^{*}\rho_{31},\\
\frac{\partial\rho_{44}}{\partial t} &= -(\Gamma_{41}+\Gamma_{42})\rho_{44}+i\Omega_{42}\rho_{24}-i\Omega_{42}^{*}\rho_{42},\\
\frac{\partial\rho_{21}}{\partial t} &= -F_{21}\rho_{21}+i\Omega_{42}^{*}\rho_{41}-i\Omega_{31}\rho_{23},\\
\frac{\partial\rho_{31}}{\partial t} &= -F_{31}\rho_{31}-i\Omega_{31}(\rho_{33}-\rho_{11}),\\
\frac{\partial\rho_{41}}{\partial t} &= -F_{41}\rho_{41}+i\Omega_{42}\rho_{21}-i\Omega_{31}\rho_{43},\\
\frac{\partial\rho_{32}}{\partial t} &= -F_{32}\rho_{32}-i\Omega_{42}\rho_{34}+i\Omega_{31}\rho_{12},\\
\frac{\partial\rho_{42}}{\partial t} &= -F_{42}\rho_{42}-i\Omega_{42}(\rho_{44}-\rho_{22}),\\
\frac{\partial\rho_{43}}{\partial t} &= -F_{43}\rho_{43}-i\Omega_{13}^{*}\rho_{41}+i\Omega_{42}\rho_{23}. \qquad (8)
\end{aligned}$$

In writing the above, we made use of the following abbreviations: $F_{21}=1/2(\Gamma_{21}+\Gamma_{12}+\gamma_{22}+\gamma_{11})+i\omega_{21}$, $F_{31}=1/2(\Gamma_{31}+\Gamma_{32}+\Gamma_{12}+\gamma_{11})+i\delta$, $F_{41}=1/2(\Gamma_{41}+\Gamma_{42}+\Gamma_{12}+\gamma_{11})+i(\delta-\omega_{34})$, $F_{32}=1/2(\Gamma_{31}+\Gamma_{32}+\Gamma_{21}+\gamma_{22})+i(\delta-\omega_{21})$, $F_{42}=1/2(\Gamma_{41}+\Gamma_{42}+\Gamma_{21}+\gamma_{22})+i(\delta-\omega_{34}-\omega_{21})$, and $F_{43}=1/2(\Gamma_{41}+\Gamma_{42}+\Gamma_{31}+\Gamma_{32})-i\omega_{34}$.

Let us define the vector $U(t)=[\rho_{22}(t),\rho_{33}(t),\rho_{44}(t),\rho_{21}(t),\rho_{12}(t),\rho_{31}(t),\rho_{13}(t),\ \rho_{41}(t),\rho_{14}(t),\rho_{32}(t),\rho_{23}(t),\rho_{42}(t),\rho_{24}(t),\rho_{43}(t),\rho_{34}(t)]^{T}$, where superscript T stands for transpose. Then we can write Eq. (8) in matrix form as

$$\frac{d}{dt}U(t)=MU(t)+B, \qquad (9)$$

with M being an (8×8) matrix and B a column vector whose coefficients can be determined from Eq. (8). Steady-state values for populations and coherences are derived through $U(\infty)=M^{-1}(-B)$.

We are interested in determining the spectral properties of the fluorescent photons, in particular the so-called resonance fluorescence spectrum (RFS) of the QDs. In the steady-state regime, this spectrum is proportional to the Fourier transformation of the correlation function $\lim_{t\to\infty}\langle E_s^{-}(r,t'+t)\cdot E_s^{+}(r,t)\rangle$, where $E_s^{-}(r,t)/E_s^{+}(r,t)$ is the negative/positive frequency part of the radiation field in the far zone. The radiation field consists of a free-field operator and a source-field operator that is proportional to the atomic polarization operator [40]. Therefore, the steady-state RFS can be expressed in terms of the atomic correlation function

$$S_m(\omega)\propto \mathrm{Re}\left[\lim_{t\to\infty}\int_0^{\infty}\langle\vec{E}_{s,m}^{-}(t'+t)\cdot\vec{E}_{s,m}^{+}(t)\rangle e^{-i\omega t'}dt'\right] \quad (m=x,y), \qquad (10)$$

where Re[ ] denotes the real part of the magnitude enclosed in square brackets, and $E_{s,m}^{-}(t)$ is the negative frequency part of the fluorescent field which in the far-field zone ($|\vec{r}|\gg c/\omega_{kj}$, $k=3,4$, $j=1,2$) reads

$$\begin{aligned}
\vec{E}_{s,x}^{-}(\vec{r},t) &= \left[\frac{\omega_{31}^2}{c^2|\vec{r}|}\vec{\mu}_{13}\sigma_{31}(t-|\vec{r}|/c)+\frac{\omega_{42}^2}{c^2|\vec{r}|}\vec{\mu}_{24}\sigma_{42}(t-|\vec{r}|/c)\right]e^{-i\omega(t-r/c)},\\
\vec{E}_{s,y}^{-}(\vec{r},t) &= \left[\frac{\omega_{32}^2}{c^2|\vec{r}|}\vec{\mu}_{23}\sigma_{32}(t-|\vec{r}|/c)+\frac{\omega_{41}^2}{c^2|\vec{r}|}\vec{\mu}_{14}\sigma_{41}(t-|\vec{r}|/c)\right]e^{-i\omega(t-r/c)}, \qquad (11)
\end{aligned}$$

and $\vec{E}_{s,m}^{+}(t)=(\vec{E}_{s,m}^{-}(t))^{\dagger}$ $(m=x,y)$. In what follows we will assume that $\omega_{31}\approx\omega_{32}\approx\omega_{41}\approx\omega_{42}$, and introduce the spatial factor $f(r)\equiv\frac{\omega_{32}^2}{c^2|\vec{r}|}$.

In writing Eq. (10), we abbreviate $\omega-\omega_L$ by ω, but we should interpret ω as a frequency measured relative to the laser frequency ω_L, since we will assume that the QD is driven by a π_x polarized laser field. The calculation of $S_{x(y)}(\omega)$ requires us to evaluate two time correlation functions, which can be performed by means of the quantum-regression theorem [40–42].

Now we may study the optical properties of light scattered by the atom, such as the spectral normally ordered field variance of E_θ or the squeezing spectrum, which was defined in Refs. [43–46] as

$$\langle:S_k(\vec{r},\omega,\theta):\rangle=\frac{1}{2\pi}\int_{-\infty}^{\infty}d\tau\, e^{-i\omega\tau}T\langle:\vec{E}_{k,\theta}(\vec{r},t),\vec{E}_{k,\theta}(\vec{r},t+\tau):\rangle \quad (k=x,y), \qquad (12)$$

where $\langle A,B\rangle=\langle A\,B\rangle-\langle A\rangle\langle B\rangle$ and T is the time ordering operator. Squeezing is characterized by the condition that the normally ordered variance $\langle:S_k(\vec{r},\omega,\theta):\rangle$ of the electric-field quadrature component $\vec{E}_{k,\theta}$ is negative. For this purpose, the operator of the electric field at the observation point $\vec{r}$ is required. We introduce the slowly varying electric-field operator with phase θ as

$$\vec{E}_{k,\theta}(\vec{r},t)=\tfrac{1}{2}\vec{E}_{s,k}^{+}(\vec{r},t)e^{i(\omega_L t+\theta)}+\tfrac{1}{2}\vec{E}_{s,k}^{-}(\vec{r},t)e^{-i(\omega_L t+\theta)} \quad (k=x,y). \qquad (13)$$

In the case of considering the π_x polarized optical transitions, we first calculate the integrand of Eq. (12),

$$\begin{aligned}
T\langle:\vec{E}_{x,\theta}(\vec{r},t_1),\vec{E}_{x,\theta}(\vec{r},t_2):\rangle &= T\langle:[\vec{E}_{s,x}^{+}(t_1)e^{i(\omega_L t_1+\theta)}+\vec{E}_{s,x}^{-}(t_1)e^{-i(\omega_L t_1+\theta)}][\vec{E}_{s,x}^{+}(t_2)e^{i(\omega_L t_2+\theta)}+\vec{E}_{s,x}^{-}(t_2)e^{-i(\omega_L t_2+\theta)}]:\rangle\\
&= T\langle:\vec{E}_{s,x}^{+}(t_1),\vec{E}_{s,x}^{+}(t_2):\rangle e^{+i(\omega_L(t_1+t_2)+2\theta)}+T\langle:\vec{E}_{s,x}^{+}(t_1),\vec{E}_{s,x}^{-}(t_2):\rangle e^{+i\omega_L(t_1-t_2)}\\
&\quad +T\langle:\vec{E}_{s,x}^{-}(t_1),\vec{E}_{s,x}^{+}(t_2):\rangle e^{-i\omega_L(t_1-t_2)}+T\langle:\vec{E}_{s,x}^{-}(t_1),\vec{E}_{s,x}^{-}(t_2):\rangle e^{-i(\omega_L(t_1+t_2)+2\theta)}. \qquad (14)
\end{aligned}$$

Now taking into account the time ordering, Eq. (14) can be recasted as

$$
\begin{aligned}
T\langle :\vec{E}_{x,\theta}(\vec{r},t_1),\vec{E}_{x,\theta}(\vec{r},t_2):\rangle &= \langle \vec{E}^{+}_{s,x}(t_1),\vec{E}^{+}_{s,x}(t_2)\rangle e^{i(\omega_L(t_1+t_2)+2\theta)}\Theta(t_1-t_2)+\langle \vec{E}^{+}_{s,x}(t_2),\vec{E}^{+}_{s,x}(t_1)\rangle e^{i(\omega_L(t_1+t_2)+2\theta)}\Theta(t_2-t_1)\\
&+\langle \vec{E}^{-}_{s,x}(t_1),\vec{E}^{-}_{s,x}(t_2)\rangle e^{-i(\omega_L(t_1+t_2)+2\theta)}\Theta(t_1-t_2)+\langle \vec{E}^{-}_{s,x}(t_2),\vec{E}^{-}_{s,x}(t_1)\rangle e^{-i(\omega_L(t_1+t_2)+2\theta)}\Theta(t_2-t_1)\\
&+\langle \vec{E}^{-}_{s,x}(t_1),\vec{E}^{+}_{s,x}(t_2)\rangle e^{i\omega_L(t_2-t_1)}[\Theta(t_1-t_2)+\Theta(t_2-t_1)]\\
&+\langle \vec{E}^{-}_{s,x}(t_2),\vec{E}^{-}_{s,x}(t_1)\rangle e^{i\omega_L(t_1-t_2)}[\Theta(t_1-t_2)+\Theta(t_2-t_1)],
\end{aligned}
\tag{15}
$$

where $\Theta(t)$ stands for the Heaviside function.

Inserting this last expression in Eq. (12), we obtain

$$
\begin{aligned}
\langle :S_x(\vec{r},\omega,\theta):\rangle = \frac{f(r)^2}{4\pi}Re\int_0^\infty d\tau(e^{i\omega\tau}+e^{-i\omega\tau})\Big[&\big(\mu_{13}^2\langle\sigma_{13}(t+\tau),\sigma_{13}(t)\rangle+\vec{\mu}_{13}\cdot\vec{\mu}_{24}\langle\sigma_{13}(t+\tau),\sigma_{24}(t)\rangle\\
&+\vec{\mu}_{13}\cdot\vec{\mu}_{24}\langle\sigma_{24}(t+\tau),\sigma_{13}(t)\rangle+\mu_{24}^2\langle\sigma_{24}(t+\tau),\sigma_{24}(t)\rangle\big)e^{i2(\theta+\omega_L r/c)}+\mu_{13}^2\langle\sigma_{31}(t+\tau),\sigma_{13}(t)\rangle\\
&+\vec{\mu}_{13}\cdot\vec{\mu}_{24}\langle\sigma_{31}(t+\tau),\sigma_{24}(t)\rangle+\vec{\mu}_{13}\cdot\vec{\mu}_{24}\langle\sigma_{42}(t+\tau),\sigma_{13}(t)\rangle+\mu_{24}^2\langle\sigma_{42}(t+\tau),\sigma_{24}(t)\rangle\Big].
\end{aligned}
\tag{16}
$$

As for the π_y polarized transitions, we arrive at the following expression:

$$
\begin{aligned}
\langle :S_y(\vec{r},\omega,\theta):\rangle = \frac{f(r)^2}{4\pi}\mathrm{Re}\int_0^\infty d\tau(e^{i\omega\tau}+e^{-i\omega\tau})\Big[&\big(\mu_{14}^2\langle\sigma_{14}(t+\tau),\sigma_{14}(t)\rangle+\vec{\mu}_{14}\cdot\vec{\mu}_{23}\langle\sigma_{14}(t+\tau),\sigma_{23}(t)\rangle\\
&+\vec{\mu}_{14}\cdot\vec{\mu}_{23}\langle\sigma_{23}(t+\tau),\sigma_{14}(t)\rangle+\mu_{23}^2\langle\sigma_{23}(t+\tau),\sigma_{23}(t)\rangle\big)e^{i2(\theta+\omega_L r/c)}+\mu_{14}^2\langle\sigma_{41}(t+\tau),\sigma_{14}(t)\rangle\\
&+\vec{\mu}_{14}\cdot\vec{\mu}_{23}\langle\sigma_{41}(t+\tau),\sigma_{23}(t)\rangle+\vec{\mu}_{14}\cdot\vec{\mu}_{23}\langle\sigma_{32}(t+\tau),\sigma_{14}(t)\rangle+\mu_{23}^2\langle\sigma_{32}(t+\tau),\sigma_{23}(t)\rangle\Big].
\end{aligned}
\tag{17}
$$

It is worth mentioning that Eq. (16) is a particular case of the general expression obtained in Ref. [47], where the effect of spontaneous generated coherence was considered; i.e., Eq. (12) in [47] reduces to Eq. (16) in the case with $p = 0$. However, the noise spectrum along the diagonal channels of Eq. (17) was not considered in Ref. [47].

III. NUMERICAL RESULTS

We consider the four levels of the electron-trion system in the Voigt geometry. The system is driven by an off-resonant π_x polarized laser field detuned by δ from the $|3\rangle \leftrightarrow |1\rangle$ transition. The excited level relaxes to both ground states with decay rates Γ_{31} and Γ_{32}. The same laser also drives the transition $|4\rangle \leftrightarrow |2\rangle$ in a more off-resonant way, which in turn results in a small pumping of population in the opposite direction with decay rates Γ_{41} and Γ_{42}. In what follows we assume that $\Gamma_{41} = \Gamma_{42} = \Gamma_{32} = \Gamma_{31} \equiv \Gamma_0 = 1.2\ \mu$eV, and we consider the g factors $g^e = -0.46$ and $g^h = -0.29$, as in Ref. [4]. Dephasing rates $\gamma_{11} = \gamma_{22} = 22$ MHz and cotunneling rates $\Gamma_{12} = \Gamma_{21} = 1.2$ MHz are taken from Ref. [8]. We also assume that transition dipole moments are equal, i.e., $\vec{\mu}_{13} = \vec{\mu}_{24}$, which in turn results in $\Omega_{13} = \Omega_{24} \equiv \Omega$.

The obtention of subnatural lines in the RFS has been experimentally shown to be feasible provided that the system is driven out of resonance [11]. On the other hand, it is well known that the RFS is related to the level of population achieved in the upper levels, thus our first step in our analysis is to determine how populations are distributed among the different levels under off-resonant excitation of the continuous wave (CW) driving field. The results obtained in the case of considering an external magnetic field of $B_{\mathrm{ext}} = 2$ T are shown in Fig. 2(a) in the case with $\delta = -5\Gamma_0$; there we can appreciate that the two upper levels almost share the same level of population while level $|2\rangle$ is highly populated at a particular Rabi frequency (Ω^-_{opt}), where optical pumping is high in spite of driving the system out of resonance. The results when the optical detuning is set to $\delta = +5\Gamma_0$ are shown in Fig. 2(b), which reveals that the off-resonant pumping of level $|2\rangle$ is less effective in this particular situation and the optimum Rabi frequency (Ω^+_{opt}) shifts to lower values, i.e., $\Omega^+_{\mathrm{opt}} < \Omega^-_{\mathrm{opt}}$. If we kept the optical detuning δ fixed and increase the external magnetic field, the previously described tendency is maintained, the main differences being (i) the higher level of population transferred to level $|2\rangle$ due to off-resonant pumping and (ii) the change in the values of the optimum Rabi frequencies.

Now we focus on the spectrum of scattered photons along the vertical and horizontal transitions. The results obtained for a moderate off-resonant driving field ($\delta = -5\Gamma_0$) are shown in Fig. 3(a): the solid curve corresponds to the spectrum of the driven transitions and is made up of the central line and two blue detuned and two red detuned sidebands, whereas the dashed curve arises from the undriven transitions and consequently it lacks from the central line and is made up of a quadruplet. The innermost sidebands of the undriven transitions are the ones that exhibit subnatural linewidth. The use of a positive detuning driving field modifies the spectral location of the sidebands, although the subnatural narrow lines are now the outermost sidebands along the undrived channels, as depicted in Fig. 3(b).

The spectral features depicted in Figs. 3(a) and 3(b) can be explained by moving to the dressed-state picture (DSP). It can be shown that the eigenvalues of the quantum system plus the coherent part of the Hamiltonian are provided by finding the roots of the polynomial

$$
+\lambda^4+b_1\lambda^3+b_2\lambda^2+b_3\lambda+b_4=0, \tag{18}
$$

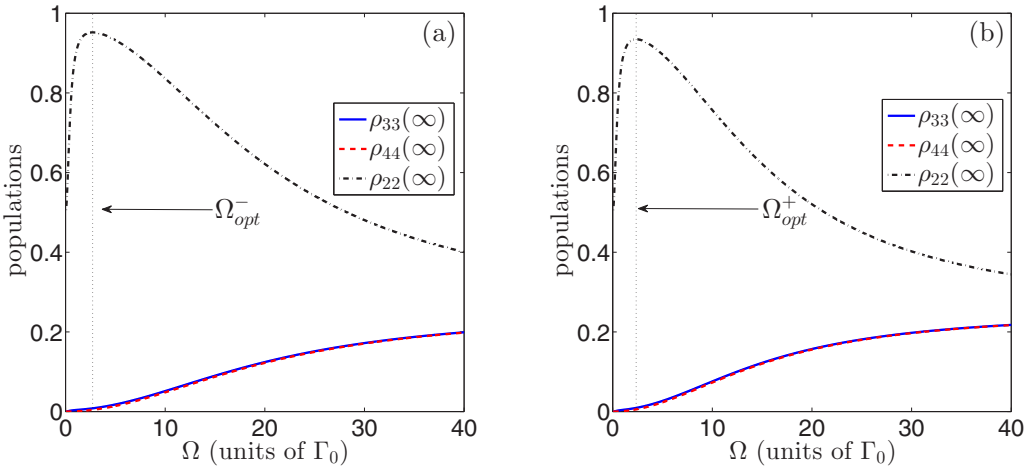

FIG. 2. Steady-state population of the states versus the Rabi frequency of the driving field Ω: $|3\rangle$ (solid curve), $|4\rangle$ (dashed curve) and $|2\rangle$ (dashed-dotted curve). Numerical values used are: $B_{\rm ext} = 2$ T, $\Gamma_0 = 1.2\mu$eV, $\gamma_{11} = \gamma_{22} = 22$ MHz, $\Gamma_{12} = \Gamma_{21} = 1.2$ MHz. (a) $\delta = -5\Gamma_0$, and (b) $\delta = +5\Gamma_0$.

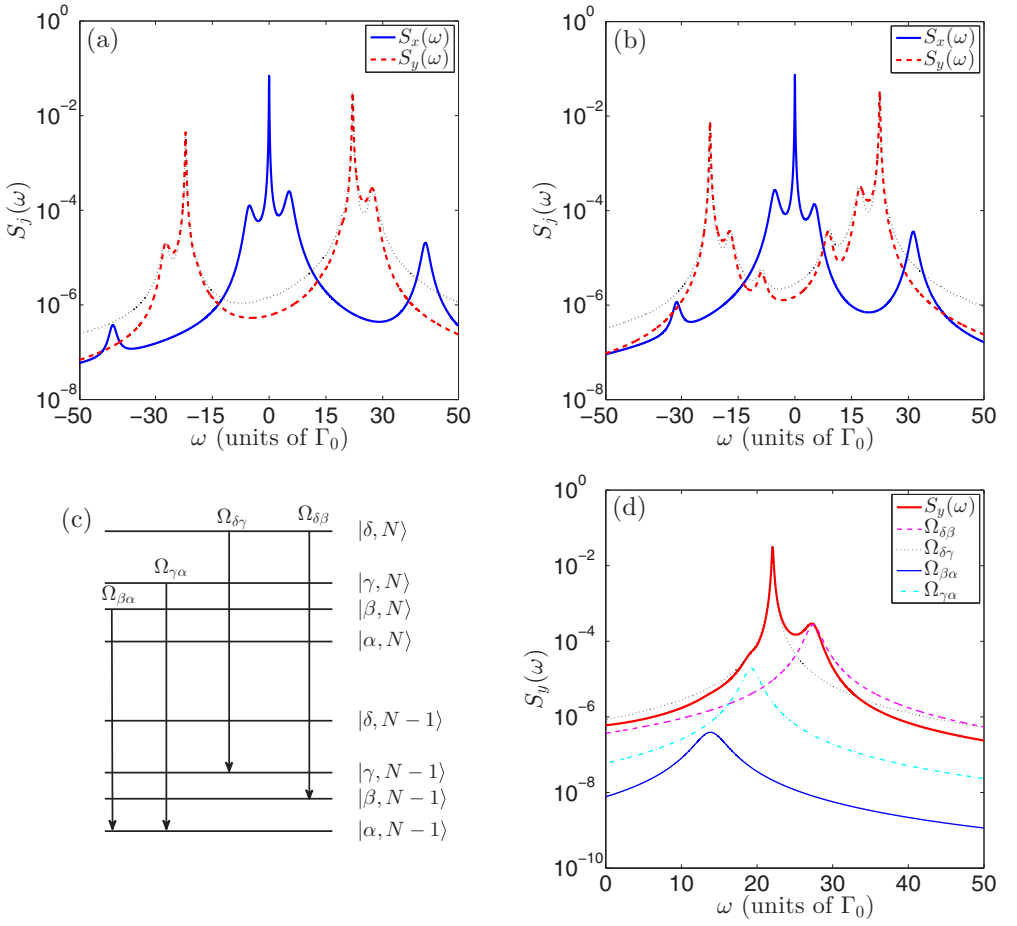

FIG. 3. Steady-state RFS of the system [$S_j(\omega)$, where $j = x, y$] driven out of resonance when $\Omega = 2\Gamma_0$: $S_x(\omega)$ (solid curve) and $S_y(\omega)$ (dashed curve). (a) $\delta = -5\Gamma_0$ and (b) $\delta = +5\Gamma_0$. The dotted curve in both panels stands for the spectrum computed in the dressed state picture [$S_y^{\rm DSP}(\omega)$] as defined in the Appendix. The rest of the parameters are as in Fig. 2. (c) Transition between dressed states accounting for the blue detuned sidebands in $S_y^{\rm DSP}(\omega)$. (d) $S_y(\omega)$ for the blue detuned sidebands depicted in (c) where $\delta = -5\Gamma_0$, and $\Omega = 2\Gamma_0$. The thin solid lines account for the different contributions in Eq. (A5).

with $b_1 = -(\omega_{21} - \omega_{34} + 2\delta)$, $b_2 = \omega_{21}\delta + (\omega_{21} + \delta)(\delta - \omega_{34}) - 2\Omega^2$, $b_3 = \Omega^2\delta + \Omega^2(\omega_{21} - \omega_{34} + \delta) - \omega_{21}\delta(\delta - \omega_{34})$, and $b_4 = \Omega^2[\Omega^2 - \omega_{21}(\delta - \omega_{34})]$. The roots are labeled as λ_j ($j = \alpha,\beta,\gamma,\delta$) and are sorted in ascending order, i.e., $\lambda_\alpha < \lambda_\beta < \lambda_\gamma < \lambda_\delta$. The corresponding eigenstates are

$$\begin{aligned} |\alpha\rangle &= a_{2\alpha}|2\rangle + a_{4\alpha}|4\rangle, \\ |\beta\rangle &= a_{1\beta}|1\rangle + a_{3\beta}|3\rangle, \\ |\gamma\rangle &= a_{1\gamma}|1\rangle + a_{3\gamma}|3\rangle, \\ |\delta\rangle &= a_{2\delta}|2\rangle + a_{4\delta}|4\rangle, \end{aligned} \tag{19}$$

where the coefficients are given by $a_{2\alpha} = +\frac{\Omega}{\sqrt{\Omega^2+(\omega_{21}-\lambda_\alpha)^2}}$, $a_{4\alpha} = +\frac{\omega_{21}-\lambda_\alpha}{\sqrt{\Omega^2+(\omega_{21}-\lambda_\alpha)^2}}$, $a_{2\delta} = -\frac{\omega_{21}-\lambda_\alpha}{\sqrt{\Omega^2+(\omega_{21}-\lambda_\alpha)^2}}$, $a_{4\delta} = +\frac{\Omega}{\sqrt{\Omega^2+(\omega_{21}-\lambda_\alpha)^2}}$, $a_{1\beta} = +\frac{\Omega}{\sqrt{\Omega^2+\lambda_\beta^2}}$, $a_{3\beta} = -\frac{\lambda_\beta}{\sqrt{\Omega^2+\lambda_\beta^2}}$, $a_{1\gamma} = +\frac{\lambda_\beta}{\sqrt{\Omega^2+\lambda_\beta^2}}$, and $a_{3\gamma} = +\frac{\Omega}{\sqrt{\Omega^2+\lambda_\beta^2}}$.

We can shed light on the features found in the spectra when considering the so-called secular approximation, which consists of obtaining equations of motion of populations and coherences while ignoring the coupling between them (the details are provided in the Appendix). Under such conditions, the spectra of photons associated with the x and y polarized channels [$S_x(\omega)$ and $S_y(\omega)$] can be split as a superposition of up to eight Lorentzians whose spectral positions are given by $\Omega_{jk} = \lambda_j - \lambda_k$ ($j,k = \alpha,\beta,\gamma,\delta$) plus the central line. Figure 3(c) shows the energy diagram of the dressed states and the transitions between adjacent manifolds, which account for all the blue detuned sidebands at a particular value of Ω and are valid for the case with $\delta < 0$.

The validity of the secular approximation can be checked by comparing the spectrum obtained using such a procedure, [$S_y^{\mathrm{DSP}}(\omega)$], with the one determined in the bare basis, [$S_y(\omega)$]. Here we can assess the closeness of the spectrum predicted in the DSP, plotted in Figs. 3(a) and 3(b) as a dotted line, to the one in the bare basis, which appears as a dashed line. In the case considered in Fig. 3(a), transitions $|\beta,N\rangle \leftrightarrow |\alpha,N-1\rangle$ and $|\gamma,N\rangle \leftrightarrow |\alpha,N-1\rangle$ have a negligible contribution and do not show up in the spectrum in the dressed basis (dotted line).

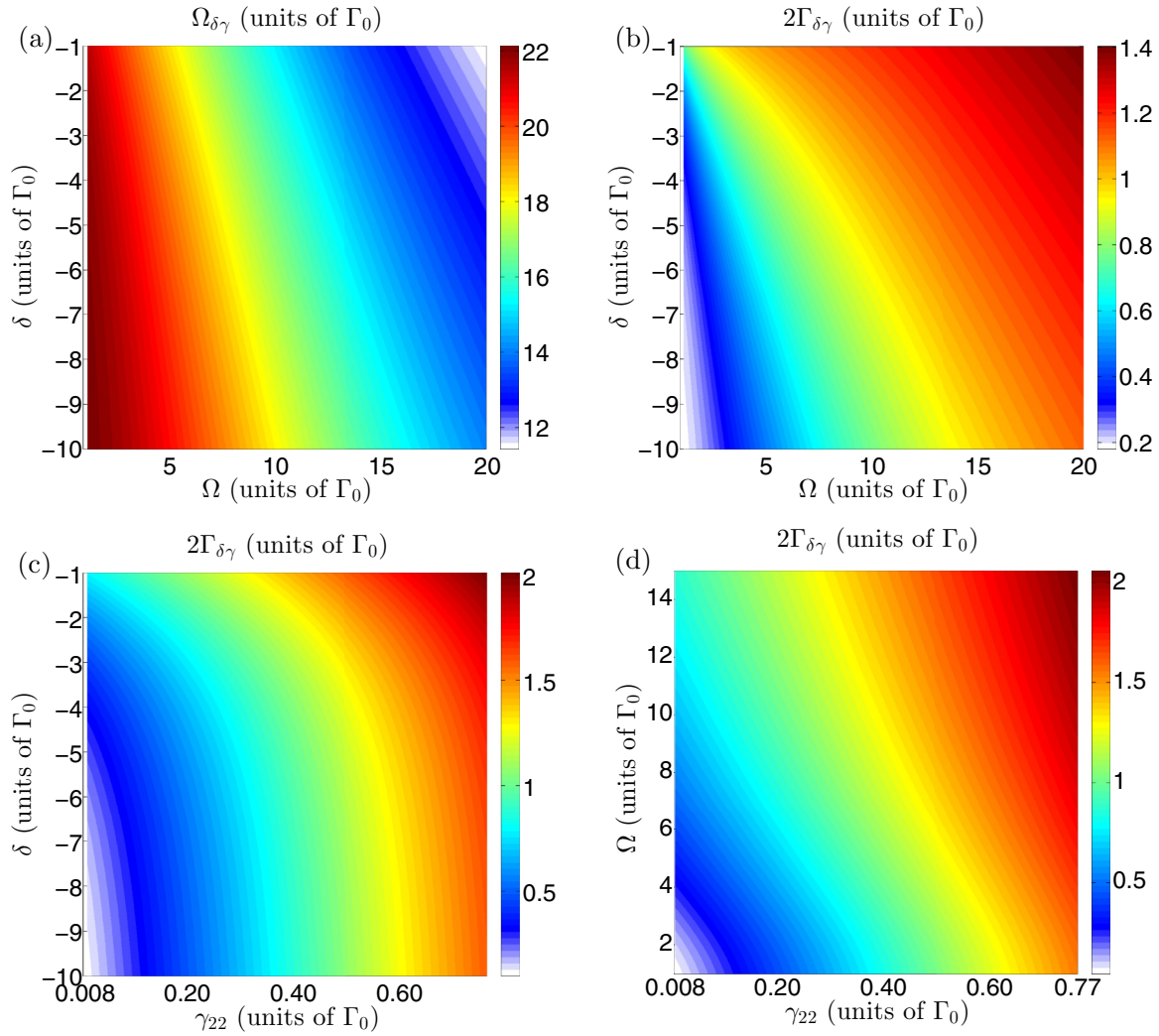

FIG. 4. (a) Spectral location of the narrow sidebands $\Omega_{\delta\gamma}$ versus the Rabi frequency Ω and the optical detuning δ. (b) Linewidth of the narrow sidebands $2\Gamma_{\delta\gamma}$ versus the Rabi frequency Ω and the optical detuning δ. (c) Linewidth of the narrow sidebands $2\Gamma_{\delta\gamma}$ versus the dephasing γ_{22} and the optical detuning δ in the case with $\Omega = 2\Gamma_0$. (d) Linewidth of the narrow sidebands $2\Gamma_{\delta\gamma}$ versus the dephasing γ_{22} and the Rabi frequency Ω in the case with $\delta = -10\Gamma_0$.

This latter effect is better appreciated in Fig. 3(d), where the individual contributions to $[S_y^{\rm DSP}(\omega)]$ are displayed separately. In addition, the subnatural narrow line is obtained along transition $|\delta,N\rangle \leftrightarrow |\gamma,N-1\rangle$, which corresponds to the inner sideband, whereas the outer sideband arises from transitions $|\delta,N\rangle \leftrightarrow |\beta,N-1\rangle$. Note that although the full spectrum along the diagonal channels (dashed curve) only shows two blue and two red detuned sidebands, the spectrum in the DSP consists of up to four blue and four red detuned sidebands [see Eq. (A5)], but two of the Lorentzians have a negligible contribution and are shadowed by the ones mentioned above.

The adequateness of the DSP to describe the RFS also holds for the case of a negative detuning, as shown with the dotted line in Fig. 3(b): in this case the Ramman photons are produced along transition $|\delta,N\rangle \leftrightarrow |\beta,N-1\rangle$ and the spectrum exhibits up to three detuned blue sidebands while the fourth one, coming from transition $|\gamma,N\rangle \leftrightarrow |\alpha,N-1\rangle$, has a vanishing contribution. Although not shown, the evaluation of $S_x(\omega)$ in the DSP $[S_x^{\rm DSP}(\omega)$ as given in Appendix] fits well the numerical findings of Figs. 3(a) and 3(b).

It is worth noting the asymmetry in the peak values of the two subnatural sidebands. This asymmetry becomes more evident for the case with negative detuning in panel 3(b) and its origin can be attributed to the the different couplings and populations of the dressed states. By picking the terms in Eq. (A4) responsible for the blue and the red detuned sidebands [which are proportional to $\langle\sigma_{\gamma\gamma}(\infty)\rangle$ and $\langle\sigma_{\delta\delta}(\infty)\rangle$, respectively], we can check that the two Lorentzians share the same linewidth but have different coefficients due to the asymmetrical coupling of the dressed states to the driving laser.

The change of either the detuning or the external magnetic field was shown to allow the frequency tuning of the Raman photons [11]. Here we show that the change of the Rabi frequency is an additional parameter which allows us to tune the center frequency of the subnatural sidebands. Figure 4(a) presents a contour plot of the center frequency $\Omega_{\delta\gamma}$ versus the Rabi frequency Ω and the optical detuning δ, while Fig. 4(b) displays the linewidth of such sidebands ($2\Gamma_{\delta\gamma}$) predicted in the DSP. These two figures indicate to us that there is a wide range of parameters (Ω,δ) which allow one to obtain subnatural Raman photons over an interval of frequencies $[14\Gamma_0, 22\Gamma_0]$. This indicates to us that the subnatural linewidth is obtained even for large pumping fields and is not dramatically modified through power broadening.

Since QDs are known to be prone to dephasing, it is essential to consider whether obtaining subnatural Raman photons is limited by this mechanism. Figure 4(c) presents a contour plot of the linewidth $2\Gamma_{\delta\gamma}$ versus the optical detuning δ and the value of γ_{22} obtained for the case with $\Omega = \Gamma_0$ and assuming that $\gamma_{11} = \gamma_{22}$. The interval of variation for γ_{22} has been taken to be from one tenth to ten times the one used in Fig. 3. Figure 4(d) presents a contour plot of the linewidth $\Gamma_{\delta\gamma}$ versus the Rabi frequency Ω and the value of γ_{22} obtained when considering an optical detuning of $\delta = -10\Gamma_0$. These two figures are useful to determine the range of parameters where subnatural photons can be obtained.

Phase-dependent spectra of the Raman photons

Another interesting aspect which, to our knowledge, has not been previously addressed relates to the level of fluctuations of the Raman photons. To this end we consider the phase-dependent spectra of the fluorescent photons produced along the diagonal transitions, $\langle: S_y(\omega,\theta) :\rangle$. We are analyzing the squeezing spectra given in Eq. (17), therefore we assume that the scattered radiation field is frequency filtered [46,48].

The most relevant finding is that the scattered field along the undriven transition exhibits reduced fluctuations at certain frequencies. Specifically, the use of a negatively/positively detuned driving field results in the obtention of squeezing at the sidebands where the Raman photons are obtained for the out-of-phase/in-phase quadrature, as shown in Fig. 5. This phenomenon has no counterpart in a two-level system, where we deal with the scattered field along the transition which is also pumped by the external laser field.

We have shown in Fig. 4(b) that the same linewidth of the Raman photons can be obtained along the $|\delta\rangle \leftrightarrow |\gamma\rangle$ transitions for different pairs of values (δ,Ω). Let us examine how the phase-dependent spectrum is modified for a selected set of pairs (δ,Ω) chosen such that $\Gamma_{\delta\gamma}$ remains constant. The results of the numerical simulations are displayed in Fig. 6(a), and indicate to us that the most favorable situation

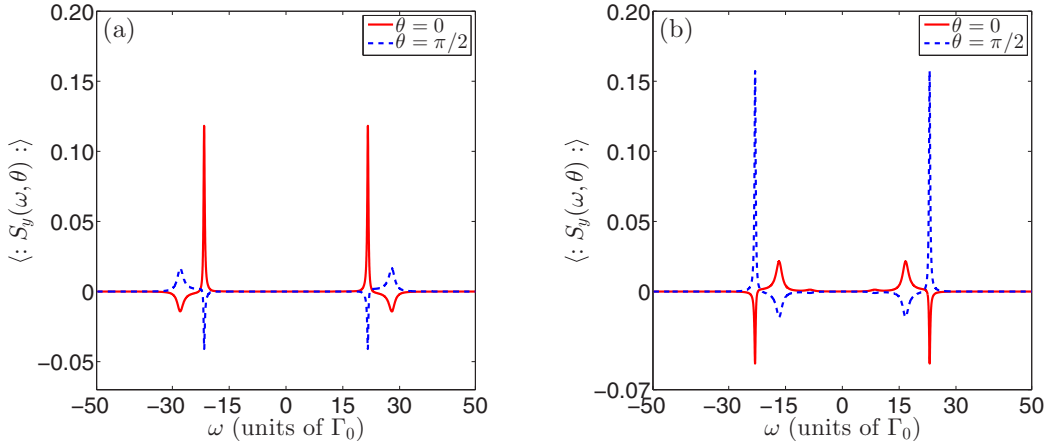

FIG. 5. Squeezing spectra for the undriven transition $\langle: S_y(\omega,\theta) :\rangle$: in phase quadrature (solid line) and out of phase quadrature (dashed line). The Rabi frequency of the field is set to $\Omega = 2\Gamma_0$, and the optical detuning to $\delta = -5\Gamma_0$ in (a) and to $\delta = +5\Gamma_0$ in (b).

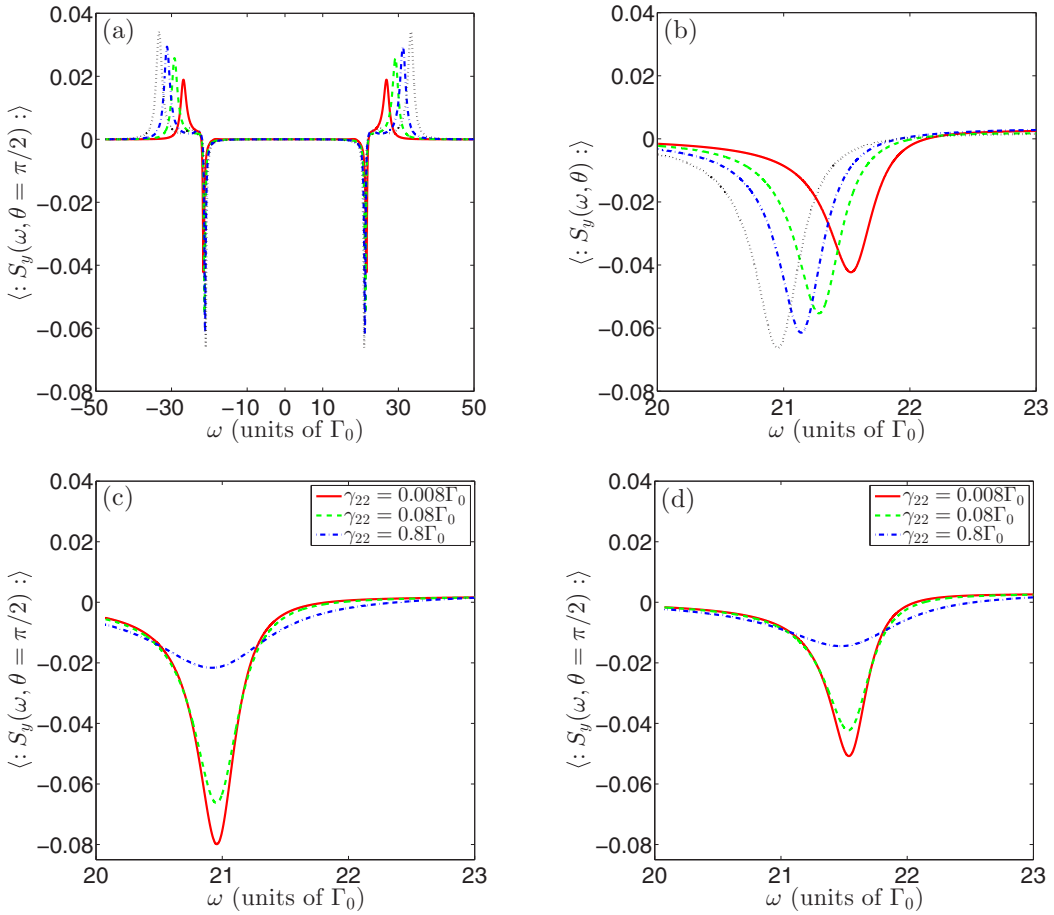

FIG. 6. (a) Squeezing spectra for the undriven transition $\langle : S_y(\omega,\theta = \pi/2) : \rangle$ for the out-of-phase quadrature for different pairs of (δ,Ω) (in units of Γ_0) such that $\Gamma_{\delta\gamma} = 0.22\Gamma_0$: $(-3.9,1.9)$ (solid curve), $(-5.8,2.8)$ (dashed curve), $(-7.4,3.4)$ (dashed-dotted curve), and $(-9.1,4.2)$ (dotted curve). Other parameters: $\gamma_{22} = 0.08\Gamma_0$. (b) Detail of panel (a) around the blue detuned sideband associated with the Raman photons. Squeezing spectra for the undriven transition $\langle : S_y(\omega,\theta = \pi/2) : \rangle$ and different values of the dephasing: $\gamma_{22} = 0.008\Gamma_0$ (solid curve), $\gamma_{22} = 0.08\Gamma_0$ (dashed curve), and $\gamma_{22} = 0.8\Gamma_0$ (dashed-dotted curve). Other parameters are (c) $\delta = -9.1\Gamma_0$ and $\Omega = 4.2\Gamma_0$; (d) $\delta = -3.9\Gamma_0$ and $\Omega = 1.9\Gamma_0$.

for maximizing the level of squeezing relies on the use of a large detuning at the expense of increasing the power of the driving field. This is better appreciated by inspecting the detailed view of the squeezing spectrum centered around the frequencies where the Raman photons are obtained, shown in Fig. 6(b).

It is to be noted that the (global) time-ordered variance or quadrature squeezing can be obtained by integrating Eq. (12) in the frequency domain [45,46,48] according to

$$\langle : (\vec{E}_{y,\theta}(\vec{r}))^2 : \rangle = \int_{-\infty}^{+\infty} d\omega \, \langle : S_y(\vec{r},\omega,\theta) : \rangle. \qquad (20)$$

The integral in Eq. (20) can be numerically computed (its analytical evaluation in the bare basis is unmanageable) and reveals that there is no quadrature squeezing for the photons produced along the diagonal transitions: $\langle : (\vec{E}_{y,\theta}(\vec{r}))^2 : \rangle > 0$. Under the secular approximation, the evaluation of Eq. (20) is straightforward using the residue theorem and confirms that the quadrature squeezing is always positive for any values of δ and Ω. It is worth noting that a recent experiment has found non-null quadrature squeezing from photons scattered from a neutral exciton transition of a single quantum dot [36].

Finally we address the question of how dephasing modifies the obtention of squeezing at the sidebands where subnatural photons can be obtained. Figure 6(c) shows the effect of dephasing rate γ_{22} on the level of squeezing obtained at the subnatural photons for the case with $\delta = -9.1\Gamma_0$ and $\Omega = 4.2\Gamma_0$. Here we can see that a reduction of the dephasing rate γ_{22} by an order of magnitude results in an increase of the negative peak value, while the increase of γ_{22} of an order of magnitude makes the peak value no longer subnatural, but fluctuations at that sideband remain negative. This behavior is obtained for other pairs of values (δ,Ω), as illustrated in Fig. 6(d).

IV. CONCLUSIONS

In this work we present a theoretical description of the spectral properties of the fluorescent photons in singly charged n-doped QDs in the Voigt geometry. The QDs are modeled as a four-level atomic system and we consider the system to be driven by a single laser field which couples the vertical transitions. The characteristics of the fluorescent photons along

the driven and the undriven channels are analyzed. When the system is driven out of resonance ($\delta \neq 0$), we show through numerical simulations that the RFS of the undriven transitions can exhibit up to two or three resolved sidebands depending on the sign of the detuning, one of them having subnatural linewidth. It is shown that the center and linewidth of such a narrow spectral line can be tuned by changing the Rabi frequency of the driving field. These spectral features are fully explained by moving to the DSP in the secular approximation, where it is shown that the RFS can be decomposed as a superposition of Lorentzians whose center, amplitudes, and linewidths account for the different numerical findings. In addition, we have determined the phase-dependent spectra of the fluorescent photons when $\delta \neq 0$, showing that under certain conditions the narrow sidebands can exhibit fluctuations below the limit set by vacuum fluctuations. The level of squeezing found is shown to depend on both the detuning and the Rabi frequency of the driving field. The influence of dephasing on the RFS and the phase-dependent spectra is also analyzed, showing that this is a limiting factor to obtain narrow spectral lines of the scattered photons along the undriven transitions.

ACKNOWLEDGMENTS

This work has been supported by Project No. FIS2013-41709-P (MICINN of Spain). F.C. acknowledges funding to MECD through Grant No. PRX16/00473, and E. Paspalakis for his hospitality.

APPENDIX: RESONANCE FLUORESCENCE AND SQUEEZING SPECTRA IN THE DRESSED STATE BASIS

To obtain the spectra we need to transform the atomic operators $\sigma_{ij}(\tau)$ $(i,j = 1,2,3,4)$ to the dressed basis through

$$\begin{aligned}\sigma_{ij}(\tau) = {} & \sigma_{\alpha\alpha}(\tau)a_{i\alpha}a_{j\alpha} + \sigma_{\beta\beta}(\tau)a_{i\beta}a_{j\beta} + \sigma_{\gamma\gamma}(\tau)a_{i\gamma}a_{j\gamma} + \sigma_{\delta\delta}(\tau)a_{i\delta}a_{j\delta} + \sigma_{\alpha\beta}(\tau)a_{i\alpha}a_{j\beta} + \sigma_{\beta\alpha}(\tau)a_{i\beta}a_{j\alpha} + \sigma_{\alpha\gamma}(\tau)a_{i\alpha}a_{j\gamma} \\ & + \sigma_{\gamma\alpha}(\tau)a_{i\gamma}a_{j\alpha} + \sigma_{\alpha\delta}(\tau)a_{i\alpha}a_{j\delta} + \sigma_{\delta\alpha}(\tau)a_{i\delta}a_{j\alpha} + \sigma_{\beta\gamma}(\tau)a_{i\beta}a_{j\gamma} + \sigma_{\gamma\beta}(\tau)a_{i\gamma}a_{j\beta} + \sigma_{\beta\delta}(\tau)a_{i\beta}a_{j\delta} + \sigma_{\delta\beta}(\tau)a_{i\delta}a_{j\beta} \\ & + \sigma_{\gamma\delta}(\tau)a_{i\gamma}a_{j\delta} + \sigma_{\delta\gamma}(\tau)a_{i\delta}a_{j\gamma}. \end{aligned} \tag{A1}$$

With the help of Eq. (A1) we can derive the equations of motion for populations and coherences in the secular approximation, which read

$$\begin{aligned}
&\frac{d\langle\sigma_{\alpha\alpha}(t)\rangle}{dt} = \hat{\Gamma}_{\alpha\alpha}\langle\sigma_{\alpha\alpha}(t)\rangle + \hat{\Gamma}_{\alpha\beta}\langle\sigma_{\beta\beta}(t)\rangle + \hat{\Gamma}_{\alpha\gamma}\langle\sigma_{\gamma\gamma}(t)\rangle + \hat{\Gamma}^0_{\alpha\alpha}, \\
&\frac{d\langle\sigma_{\beta\beta}(t)\rangle}{dt} = \hat{\Gamma}_{\beta\alpha}\langle\sigma_{\alpha\alpha}(t)\rangle + \hat{\Gamma}_{\beta\beta}\langle\sigma_{\beta\beta}(t)\rangle + \hat{\Gamma}_{\beta\gamma}\langle\sigma_{\gamma\gamma}(t)\rangle + \hat{\Gamma}^0_{\beta\beta}, \\
&\frac{d\langle\sigma_{\gamma\gamma}(t)\rangle}{dt} = \hat{\Gamma}_{\gamma\alpha}\langle\sigma_{\alpha\alpha}(t)\rangle + \hat{\Gamma}_{\gamma\beta}\langle\sigma_{\beta\beta}(t)\rangle + \hat{\Gamma}_{\gamma\gamma}\langle\sigma_{\gamma\gamma}(t)\rangle + \hat{\Gamma}^0_{\gamma\gamma}, \\
&\frac{d\langle\sigma_{\beta\alpha}(t)\rangle}{dt} = -(\Gamma_{\beta\alpha} - i\Omega_{\beta\alpha})\langle\sigma_{\beta\alpha}(t)\rangle, \quad \frac{d\langle\sigma_{\gamma\alpha}(t)\rangle}{dt} = -(\Gamma_{\gamma\alpha} - i\Omega_{\gamma\alpha})\langle\sigma_{\gamma\alpha}(t)\rangle, \\
&\frac{d\langle\sigma_{\alpha\delta}(t)\rangle}{dt} = -(\Gamma_{\alpha\delta} - i\Omega_{\alpha\delta})\langle\sigma_{\alpha\delta}(t)\rangle, \quad \frac{d\langle\sigma_{\beta\gamma}(t)\rangle}{dt} = -(\Gamma_{\beta\gamma} - i\Omega_{\beta\gamma})\langle\sigma_{\beta\gamma}(t)\rangle, \\
&\frac{d\langle\sigma_{\beta\delta}(t)\rangle}{dt} = -(\Gamma_{\beta\delta} - i\Omega_{\beta\delta})\langle\sigma_{\beta\delta}(t)\rangle, \quad \frac{d\langle\sigma_{\gamma\delta}(t)\rangle}{dt} = -(\Gamma_{\gamma\delta} - i\Omega_{\gamma\delta})\langle\sigma_{\gamma\delta}(t)\rangle,
\end{aligned} \tag{A2}$$

where $\Omega_{jk} = \lambda_j - \lambda_k$ ($j \neq k$ and $j,k = \alpha,\beta,\gamma,\delta$) stands for the effective Rabi frequencies in the new basis, and the coefficients appearing in Eq. (A2) involving populations read

$$\begin{aligned}
&\hat{\Gamma}^0_{\alpha\alpha} = +\Gamma_{42}a^2_{2\alpha}a^2_{4\delta} + \gamma_{22}a^2_{2\alpha}a^2_{2\delta}, \\
&\hat{\Gamma}_{\alpha\alpha} = -(\Gamma_{42}+\Gamma_{41})a^2_{4\alpha} - (\Gamma_{21}+\gamma_{22})a^2_{2\alpha} - \gamma_{22}a^2_{2\alpha} - \gamma_{22}a^2_{2\alpha}a^2_{2\delta} - \Gamma_{42}a^2_{2\alpha}a^2_{4\delta} + \Gamma_{42}a^2_{2\alpha}a^2_{4\alpha} + \gamma_{22}a^4_{2\alpha}, \\
&\hat{\Gamma}_{\alpha\beta} = \Gamma_{32}a^2_{2\alpha}a^2_{3\beta} + \Gamma_{12}a^2_{1\beta}a^2_{2\alpha} - \Gamma_{42}a^2_{2\alpha}a^2_{4\delta} - \gamma_{22}a^2_{2\alpha}a^2_{2\delta}, \quad \hat{\Gamma}_{\alpha\gamma} = \Gamma_{32}a^2_{2\alpha}a^2_{3\gamma} + \Gamma_{12}a^2_{1\gamma}a^2_{2\alpha} - \Gamma_{42}a^2_{2\alpha}a^2_{4\delta} - \gamma_{22}a^2_{2\alpha}a^2_{2\delta}, \\
&\hat{\Gamma}^0_{\beta\beta} = +\Gamma_{41}a^2_{1\beta}a^2_{4\delta} + \Gamma_{21}a^2_{1\beta}a^2_{2\delta}, \quad \hat{\Gamma}_{\beta\alpha} = \Gamma_{41}a^2_{1\beta}a^2_{4\alpha} + \Gamma_{21}a^2_{1\beta}a^2_{2\alpha} - \Gamma_{41}a^2_{1\beta}a^2_{4\delta} - \Gamma_{21}a^2_{1\beta}a^2_{2\delta}, \\
&\hat{\Gamma}_{\beta\beta} = -(\Gamma_{32}+\Gamma_{31})a^2_{3\beta} - (\Gamma_{12}+\gamma_{11})a^2_{1\beta} - \Gamma_{21}a^2_{1\beta}a^2_{2\delta} - \Gamma_{41}a^2_{1\beta}a^2_{4\delta} + \Gamma_{31}a^2_{1\beta}a^2_{3\beta} + \gamma_{11}a^4_{4\beta}, \\
&\hat{\Gamma}_{\beta\gamma} = \Gamma_{31}a^2_{1\beta}a^2_{3\gamma} + \gamma_{11}a^2_{1\beta}a^2_{1\gamma} - \Gamma_{41}a^2_{1\beta}a^2_{4\delta} - \Gamma_{21}a^2_{1\beta}a^2_{2\delta}, \quad \hat{\Gamma}^0_{\gamma\gamma} = +\Gamma_{41}a^2_{1\gamma}a^2_{4\delta} + \Gamma_{21}a^2_{1\gamma}a^2_{2\delta}, \\
&\hat{\Gamma}_{\gamma\alpha} = \Gamma_{41}a^2_{1\gamma}a^2_{4\alpha} + \Gamma_{21}a^2_{1\gamma}a^2_{2\alpha} - \Gamma_{41}a^2_{1\gamma}a^2_{4\delta} - \Gamma_{21}a^2_{1\gamma}a^2_{2\delta}, \quad \hat{\Gamma}_{\gamma\beta} = \Gamma_{31}a^2_{1\gamma}a^2_{3\beta} + \gamma_{11}a^2_{1\beta}a^2_{1\gamma} - \Gamma_{41}a^2_{1\gamma}a^2_{4\delta} - \Gamma_{21}a^2_{1\gamma}a^2_{2\delta}, \\
&\hat{\Gamma}_{\gamma\gamma} = -(\Gamma_{32}+\Gamma_{31})a^2_{3\gamma} - (\Gamma_{12}+\gamma_{11})a^2_{1\gamma} - \Gamma_{21}a^2_{1\gamma}a^2_{2\delta} - \Gamma_{41}a^2_{1\gamma}a^2_{4\delta} + \Gamma_{31}a^2_{1\gamma}a^2_{3\gamma} + \gamma_{11}a^4_{1\gamma},
\end{aligned} \tag{A3}$$

whereas the coefficients appearing in Eq. (A2) involving coherences read

$$\begin{aligned}
\Gamma_{\beta\alpha} &= \frac{\Gamma_{32}+\Gamma_{31}}{2}a_{3\beta}^2 + \frac{\Gamma_{42}+\Gamma_{41}}{2}a_{4\alpha}^2 + \frac{\Gamma_{21}+\gamma_{22}}{2}a_{2\alpha}^2 + \frac{\Gamma_{12}+\gamma_{11}}{2}a_{1\beta}^2,\\
\Gamma_{\gamma\alpha} &= \frac{\Gamma_{32}+\Gamma_{31}}{2}a_{3\gamma}^2 + \frac{\Gamma_{42}+\Gamma_{41}}{2}a_{4\alpha}^2 + \frac{\Gamma_{21}+\gamma_{22}}{2}a_{2\alpha}^2 + \frac{\Gamma_{12}+\gamma_{11}}{2}a_{1\gamma}^2,\\
\Gamma_{\alpha\delta} &= \frac{\Gamma_{41}+\Gamma_{42}}{2}\left(a_{4\alpha}^2+a_{4\delta}^2\right) + \frac{\Gamma_{21}+\gamma_{22}}{2}\left(a_{2\alpha}^2+a_{2\delta}^2\right) - \gamma_{22}a_{2\alpha}^2a_{2\delta}^2 - \Gamma_{42}a_{2\alpha}a_{2\delta}a_{4\alpha}a_{4\delta},\\
\Gamma_{\beta\gamma} &= \frac{\Gamma_{31}+\Gamma_{32}}{2}\left(a_{3\beta}^2+a_{3\gamma}^2\right) + \frac{\Gamma_{12}+\gamma_{11}}{2}\left(a_{1\beta}^2+a_{1\gamma}^2\right) - \gamma_{11}a_{1\gamma}^2a_{1\beta}^2 - \Gamma_{31}a_{1\beta}a_{1\gamma}a_{3\beta}a_{3\gamma},\\
\Gamma_{\beta\delta} &= \frac{\Gamma_{32}+\Gamma_{31}}{2}a_{3\beta}^2 + \frac{\Gamma_{42}+\Gamma_{41}}{2}a_{4\delta}^2 + \frac{\Gamma_{21}+\gamma_{22}}{2}a_{2\delta}^2 + \frac{\Gamma_{12}+\gamma_{11}}{2}a_{1\beta}^2,\\
\Gamma_{\gamma\delta} &= \frac{\Gamma_{32}+\Gamma_{31}}{2}a_{3\gamma}^2 + \frac{\Gamma_{42}+\Gamma_{41}}{2}a_{4\delta}^2 + \frac{\Gamma_{21}+\gamma_{22}}{2}a_{2\delta}^2 + \frac{\Gamma_{12}+\gamma_{11}}{2}a_{1\gamma}^2.
\end{aligned} \tag{A4}$$

The RFS spectra along the diagonal and vertical channels in the DSP are derived by making use of Eq. (A2), and the final results read as

$$\begin{aligned}
S_y^{\mathrm{DSP}}(\omega) \approx {} & +a_{3\beta}^2a_{2\alpha}^2\frac{\Gamma_{\beta\alpha}\langle\sigma_{\beta\beta}(\infty)\rangle}{\Gamma_{\beta\alpha}^2+(\omega+\Omega_{\beta\alpha})^2} + a_{1\beta}^2a_{4\alpha}^2\frac{\Gamma_{\beta\alpha}\langle\sigma_{\alpha\alpha}(\infty)\rangle}{\Gamma_{\beta\alpha}^2+(\omega-\Omega_{\beta\alpha})^2} + a_{1\beta}^2a_{4\delta}^2\frac{\Gamma_{\beta\delta}\langle\sigma_{\delta\delta}(\infty)\rangle}{\Gamma_{\beta\delta}^2+(\omega+\Omega_{\beta\delta})^2} + a_{3\beta}^2a_{2\delta}^2\frac{\Gamma_{\beta\delta}\langle\sigma_{\beta\beta}(\infty)\rangle}{\Gamma_{\beta\delta}^2+(\omega-\Omega_{\beta\delta})^2}\\
& + a_{3\gamma}^2a_{2\alpha}^2\frac{\Gamma_{\gamma\alpha}\langle\sigma_{\gamma\gamma}(\infty)\rangle}{\Gamma_{\gamma\alpha}^2+(\omega+\Omega_{\gamma\alpha})^2} + a_{1\gamma}^2a_{4\alpha}^2\frac{\Gamma_{\gamma\alpha}\langle\sigma_{\alpha\alpha}(\infty)\rangle}{\Gamma_{\gamma\alpha}^2+(\omega-\Omega_{\gamma\alpha})^2} + a_{1\gamma}^2a_{4\delta}^2\frac{\Gamma_{\gamma\delta}\langle\sigma_{\delta\delta}(\infty)\rangle}{\Gamma_{\gamma\delta}^2+(\omega+\Omega_{\gamma\delta})^2} + a_{3\gamma}^2a_{2\delta}^2\frac{\Gamma_{\gamma\delta}\langle\sigma_{\gamma\gamma}(\infty)\rangle}{\Gamma_{\gamma\delta}^2+(\omega-\Omega_{\gamma\delta})^2},
\end{aligned} \tag{A5}$$

$$\begin{aligned}
S_x^{\mathrm{DSP}}(\omega) \approx {} & +a_{3\beta}^2a_{1\gamma}^2\frac{\Gamma_{\beta\gamma}\langle\sigma_{\beta\beta}(\infty)\rangle}{\Gamma_{\beta\gamma}^2+(\omega+\Omega_{\beta\gamma})^2} + a_{3\gamma}^2a_{1\beta}^2\frac{\Gamma_{\beta\gamma}\langle\sigma_{\gamma\gamma}(\infty)\rangle}{\Gamma_{\beta\gamma}^2+(\omega-\Omega_{\beta\gamma})^2} + a_{4\alpha}^2a_{2\delta}^2\frac{\Gamma_{\alpha\delta}\langle\sigma_{\alpha\alpha}(\infty)\rangle}{\Gamma_{\alpha\delta}^2+(\omega+\Omega_{\alpha\delta})^2}\\
& + a_{4\delta}^2a_{2\alpha}^2\frac{\Gamma_{\alpha\delta}\langle\sigma_{\delta\delta}(\infty)\rangle}{\Gamma_{\alpha\delta}^2+(\omega-\Omega_{\alpha\delta})^2} + S_{0,x}(\omega),
\end{aligned} \tag{A6}$$

where the term $S_{0,x}(\omega)$ accounts for transitions between adjacent manifolds of dressed states, i.e., from $|j,N\rangle$ to $|j,N-1\rangle$ ($j=\alpha,\beta,\gamma,\delta$), thus the frequency of these transitions is located at ω_L.

To determine the contributions to the central line $S_{0,x}(\omega)$, let us define the vector $U_{jj}(\tau) = [\langle\sigma_{\alpha\alpha}(\tau),\sigma_{jj}(0)\rangle,\langle\sigma_{\beta\beta}(\tau),\sigma_{jj}(0),\langle\sigma_{\gamma\gamma}(\tau),\sigma_{jj}(0)\rangle\rangle]$ ($j=\alpha,\beta,\gamma,\delta$). According to the quantum regression theorem and taking into account the Bloch equations for populations appearing in Eq. (A2), the vector $U_{jj}(\tau)$ satisfies the following equation:

$$\frac{d\,U_{jj}(\tau)}{d\tau} = \hat{M}U_{jj}(\tau), \tag{A7}$$

where the matrix $\hat{M}$ is given by

$$\hat{M} = \begin{pmatrix} \hat{\Gamma}_{\alpha\alpha} & \hat{\Gamma}_{\alpha\beta} & \hat{\Gamma}_{\alpha\gamma} \\ \hat{\Gamma}_{\beta\alpha} & \hat{\Gamma}_{\beta\beta} & \hat{\Gamma}_{\beta\gamma} \\ \hat{\Gamma}_{\gamma\alpha} & \hat{\Gamma}_{\gamma\beta} & \hat{\Gamma}_{\gamma\gamma} \end{pmatrix}. \tag{A8}$$

By making use of the Laplace transform of Eq. (A7), we arrive at $U_{jj}(s) = (sI_3 - \hat{M})^{-1}[U_{jj}(0)]$, I_3 being a 3×3 identity matrix, where we should make the replacement $s = i\omega$. Finally the contributions to the central line read

$$S_{0,x}(\omega) = \mathrm{Re}\Big[+ a_{2\alpha}^2a_{4\alpha}^2U_{\alpha\alpha}^{(1)}(i\omega) + a_{3\beta}^2a_{1\beta}^2U_{\beta\beta}^{(2)}(i\omega) + a_{3\gamma}^2a_{1\gamma}^2U_{\gamma\gamma}^{(3)}(i\omega) - a_{2\delta}^2a_{4\delta}^2\left(U_{\delta\delta}^{(1)}(i\omega) + U_{\delta\delta}^{(2)}(i\omega) + U_{\delta\delta}^{(3)}(i\omega)\right)\Big], \tag{A9}$$

where $U_{jj}^{(k)}(i\omega)$ stands for the kth element of vector $U_{jj}(i\omega)$.

The squeezing spectra along the diagonal and vertical channels in the DSP are derived by making use of Eq. (A2), and the final results for the in phase cuadrature read as

$$\begin{aligned}
\left\langle : S_y^{\mathrm{DSP}}(\omega,\theta=0) : \right\rangle = {} & +\frac{\Gamma_{\beta\alpha}}{\Gamma_{\beta\alpha}^2+(\omega\pm\Omega_{\beta\alpha})^2}\left[a_{2\alpha}^2a_{3\beta}^2\langle\sigma_{\beta\beta}(\infty)\rangle + a_{1\beta}^2a_{4\alpha}^2\langle\sigma_{\alpha\alpha}(\infty)\rangle + a_{1\beta}a_{3\beta}a_{2\alpha}a_{4\alpha}(\langle\sigma_{\alpha\alpha}(\infty)\rangle + \langle\sigma_{\beta\beta}(\infty)\rangle)\right]\\
& + \frac{\Gamma_{\delta\beta}}{\Gamma_{\delta\beta}^2+(\omega\pm\Omega_{\delta\beta})^2}\left[a_{2\delta}^2a_{3\beta}^2\langle\sigma_{\beta\beta}(\infty)\rangle + a_{1\beta}^2a_{4\delta}^2\langle\sigma_{\delta\delta}(\infty)\rangle + a_{1\beta}a_{3\beta}a_{2\delta}a_{4\delta}(\langle\sigma_{\delta\delta}(\infty)\rangle + \langle\sigma_{\beta\beta}(\infty)\rangle)\right]
\end{aligned}$$

$$+\frac{\Gamma_{\gamma\alpha}}{\Gamma_{\gamma\alpha}^2+(\omega\pm\Omega_{\gamma\alpha})^2}\left[a_{1\gamma}^2a_{4\alpha}^2\langle\sigma_{\alpha\alpha}(\infty)\rangle+a_{2\alpha}^2a_{3\gamma}^2\langle\sigma_{\gamma\gamma}(\infty)\rangle+a_{1\gamma}a_{3\gamma}a_{2\alpha}a_{4\alpha}(\langle\sigma_{\alpha\alpha}(\infty)\rangle+\langle\sigma_{\gamma\gamma}(\infty)\rangle)\right]$$
$$+\frac{\Gamma_{\delta\gamma}}{\Gamma_{\delta\gamma}^2+(\omega\pm\Omega_{\delta\gamma})^2}\left[a_{1\gamma}^2a_{4\delta}^2\langle\sigma_{\delta\delta}(\infty)\rangle+a_{2\delta}^2a_{3\gamma}^2\langle\sigma_{\gamma\gamma}(\infty)\rangle+a_{1\gamma}a_{3\gamma}a_{2\delta}a_{4\delta}(\langle\sigma_{\delta\delta}(\infty)\rangle+\langle\sigma_{\gamma\gamma}(\infty)\rangle)\right], \tag{A10}$$

$$\langle:S_x^{\mathrm{DSP}}(\omega,\theta=0):\rangle=+\frac{\Gamma_{\alpha\delta}}{\Gamma_{\alpha\delta}^2+(\omega\pm\Omega_{\alpha\delta})^2}\left[a_{2\delta}^2a_{4\alpha}^2\langle\sigma_{\alpha\alpha}(\infty)\rangle+a_{2\alpha}^2a_{4\delta}^2\langle\sigma_{\delta\delta}(\infty)\rangle+a_{2\alpha}a_{2\delta}a_{4\alpha}a_{4\delta}(\langle\sigma_{\alpha\alpha}(\infty)\rangle+\langle\sigma_{\delta\delta}(\infty)\rangle)\right]$$
$$+\frac{\Gamma_{\beta\gamma}}{\Gamma_{\beta\gamma}^2+(\omega\pm\Omega_{\beta\gamma})^2}\left[a_{1\gamma}^2a_{3\beta}^2\langle\sigma_{\beta\beta}(\infty)\rangle+a_{1\beta}^2a_{3\gamma}^2\langle\sigma_{\gamma\gamma}(\infty)\rangle+a_{1\beta}a_{1\gamma}a_{3\beta}a_{3\gamma}(\langle\sigma_{\beta\beta}(\infty)\rangle+\langle\sigma_{\gamma\gamma}(\infty)\rangle)\right]$$
$$+S_x^0(\omega), \tag{A11}$$

$S_x^0(\omega)$ being the contribution to the central line. The expression for this component obeys the equation

$$S_x^0(\omega)=\mathrm{Re}\big[+2a_{2\alpha}^2a_{4\alpha}^2\big(U_{\alpha\alpha}^{(1)}(i\omega)+U_{\alpha\alpha}^{(1)}(-i\omega)\big)+2a_{3\beta}^2a_{1\beta}^2\big(U_{\beta\beta}^{(2)}(i\omega)+U_{\beta\beta}^{(2)}(-i\omega)\big)+2a_{3\gamma}^2a_{1\gamma}^2\big(U_{\gamma\gamma}^{(3)}(i\omega)+U_{\gamma\gamma}^{(3)}(-i\omega)\big)$$
$$-2a_{2\delta}^2a_{4\delta}^2\big(U_{\delta\delta}^{(1)}(i\omega)+U_{\delta\delta}^{(2)}(i\omega)+U_{\delta\delta}^{(3)}(i\omega)+U_{\delta\delta}^{(1)}(-i\omega)+U_{\delta\delta}^{(2)}(-i\omega)+U_{\delta\delta}^{(3)}(-i\omega)\big)\big]. \tag{A12}$$

The formulas for the out-of-phase quadrature reduce to

$$\langle:S_y^{\mathrm{DSP}}(\omega,\theta=\pi/2):\rangle=+\frac{\Gamma_{\beta\alpha}}{\Gamma_{\beta\alpha}^2+(\omega\pm\Omega_{\beta\alpha})^2}\left[a_{2\alpha}^2a_{3\beta}^2\langle\sigma_{\beta\beta}(\infty)\rangle+a_{1\beta}^2a_{4\alpha}^2\langle\sigma_{\alpha\alpha}(\infty)\rangle-a_{1\beta}a_{3\beta}a_{2\alpha}a_{4\alpha}(\langle\sigma_{\alpha\alpha}(\infty)\rangle+\langle\sigma_{\beta\beta}(\infty)\rangle)\right]$$
$$+\frac{\Gamma_{\delta\beta}}{\Gamma_{\delta\beta}^2+(\omega\pm\Omega_{\delta\beta})^2}\left[a_{2\delta}^2a_{3\beta}^2\langle\sigma_{\beta\beta}(\infty)\rangle+a_{1\beta}^2a_{4\delta}^2\langle\sigma_{\delta\delta}(\infty)\rangle-a_{1\beta}a_{3\beta}a_{2\delta}a_{4\delta}(\langle\sigma_{\delta\delta}(\infty)\rangle+\langle\sigma_{\beta\beta}(\infty)\rangle)\right]$$
$$+\frac{\Gamma_{\gamma\alpha}}{\Gamma_{\gamma\alpha}^2+(\omega\pm\Omega_{\gamma\alpha})^2}\left[a_{1\gamma}^2a_{4\alpha}^2\langle\sigma_{\alpha\alpha}(\infty)\rangle+a_{2\alpha}^2a_{3\gamma}^2\langle\sigma_{\gamma\gamma}(\infty)\rangle-a_{1\gamma}a_{3\gamma}a_{2\alpha}a_{4\alpha}(\langle\sigma_{\alpha\alpha}(\infty)\rangle+\langle\sigma_{\gamma\gamma}(\infty)\rangle)\right]$$
$$+\frac{\Gamma_{\delta\gamma}}{\Gamma_{\delta\gamma}^2+(\omega\pm\Omega_{\delta\gamma})^2}\left[a_{1\gamma}^2a_{4\delta}^2\langle\sigma_{\delta\delta}(\infty)\rangle+a_{2\delta}^2a_{3\gamma}^2\langle\sigma_{\gamma\gamma}(\infty)\rangle-a_{1\gamma}a_{3\gamma}a_{2\delta}a_{4\delta}(\langle\sigma_{\delta\delta}(\infty)\rangle+\langle\sigma_{\gamma\gamma}(\infty)\rangle)\right], \tag{A13}$$

$$\langle:S_x^{\mathrm{DSP}}(\omega,\theta=\pi/2):\rangle=+\frac{\Gamma_{\alpha\delta}}{\Gamma_{\alpha\delta}^2+(\omega\pm\Omega_{\alpha\delta})^2}\left[a_{2\delta}^2a_{4\alpha}^2\langle\sigma_{\alpha\alpha}(\infty)\rangle+a_{2\alpha}^2a_{4\delta}^2\langle\sigma_{\delta\delta}(\infty)\rangle-a_{2\alpha}a_{2\delta}a_{4\alpha}a_{4\delta}(\langle\sigma_{\alpha\alpha}(\infty)\rangle+\langle\sigma_{\delta\delta}(\infty)\rangle)\right]$$
$$+\frac{\Gamma_{\beta\gamma}}{\Gamma_{\beta\gamma}^2+(\omega\pm\Omega_{\beta\gamma})^2}\left[a_{1\gamma}^2a_{3\beta}^2\langle\sigma_{\beta\beta}(\infty)\rangle+a_{1\beta}^2a_{3\gamma}^2\langle\sigma_{\gamma\gamma}(\infty)\rangle-a_{1\beta}a_{1\gamma}a_{3\beta}a_{3\gamma}(\langle\sigma_{\beta\beta}(\infty)\rangle\right.$$
$$\left.+\langle\sigma_{\gamma\gamma}(\infty)\rangle)\right]. \tag{A14}$$

Note that in the secular approximation the out-of-phase quadrature for the spectrum corresponding to the vertical transitions lacks the central component.

[1] N. H. Bonadeo, J. Erland, D. Gammon, D. Park, D. S. Parker, and D. G. Steel, Science **282**, 1473 (1998).

[2] M. Atatüre J. Dreiser, A. Badolato, A. Högele, K. Karrai, and A. Imamoglu, Science **312**, 551 (2006).

[3] X. Xu, Y. Wu, B. Sun, Q. Huang, J. Cheng, D. G. Steel, A. S. Bracker, D. Gammon, C. Emary, and L. J. Sham, Phys. Rev. Lett. **99**, 097401 (2007).

[4] C. Emary, X. Xu, D. G. Steel, S. Saikin, and L. J. Sham, Phys. Rev. Lett. **98**, 047401 (2007).

[5] V. Loo, L. Lanco, O. Krebs, P. Senellart, and P. Voisin, Phys. Rev. B **83**, 033301 (2011).

[6] B. D. Gerardot, D. Brunner, P. A. Dalgarno, P. Öhberg, S. Seidl, M. Kroner, K. Karrai, N. G. Stoltz, P. M. Petroff, and R. J. Warburton, Nature (London) **451**, 441 (2008).

[7] A. Muller, E. B. Flagg, P. Bianucci, X. Y. Wang, D. G. Deppe, W. Ma, J. Zhang, G. J. Salamo, M. Xiao, and C. K. Shih, Phys. Rev. Lett. **99**, 187402 (2007).

[8] M. Kroner, K. M. Weiss, B. Biedermann, S. Seidl, A. W. Holleitner, A. Badolato, P. M. Petroff, P. Öhberg, R. J. Warburton, and K. Karrai, Phys. Rev. B **78**, 075429 (2008).

[9] A. N. Vamivakas, Y. Zhao, Chao-Yang Lu, and M. Atatüre, Nat. Phys. **5**, 198 (2009).

[10] E. B. Flagg, A. Muller, J. W. Robertson, S. Founta, D. G. Deppe, M. Xiao, W. Ma, G. J. Salamo, and C. K. Shih, Nat. Phys. **5**, 203 (2009).

[11] G. Fernandez, T. Volz, R. Desbuquois, A. Badolato, and A. Imamoglu, Phys. Rev. Lett. **103**, 087406 (2009).

[12] S. T. Yilmaz, P. Fallahi, and A. Imamoglu, Phys. Rev. Lett. **105**, 033601 (2010).
[13] P. Fallahi, S. T. Yilmaz, and A. Imamoglu, Phys. Rev. Lett. **105**, 257402 (2010).
[14] C.-Y. Lu, Y. Zhao, A. N. Vamivakas, C. Matthiesen, S. Fält, A. Badolato, and M. Atatüre, Phys. Rev. B **81**, 035332 (2010).
[15] G.-X. Li, S.-P. Wu, and J.-P. Zhu, J. Opt. Soc. Am. B **27**, 1634 (2010).
[16] C. Matthiesen, A. N. Vamivakas, and M. Atatüre, Phys. Rev. Lett. **108**, 093602 (2012).
[17] J. R. Schaibley, A. P. Burgers, G. A. McCracken, D. G. Steel, A. S. Bracker, D. Gammon, and L. J. Sham, Phys. Rev. B **87**, 115311 (2013).
[18] A. Ulhaq, S. Weiler, C. Roy, S. M. Ulrich, M. Jetter, S. Hugues, and P. Michler, Opt. Express **21**, 4382 (2013).
[19] R.-C. Ge, S. Weiler, A. Ulhaq, S. M. Ulrich, M. Jetter, P. Michler, and S. Hugues, Opt. Lett. **38**, 1691 (2013).
[20] K. Konthasinghe, M. Peiris, B. Petrak, Y. Yu, Z. C. Niu, and A. Muller, Opt. Lett. **40**, 1846 (2015).
[21] Z. Sun, A. Delteil, S. Faelt, and A. Imamoglu, Phys. Rev. B **93**, 241302 (2016).
[22] J. M. Zajac and S. I. Erlingsson, Phys. Rev. B **94**, 035432 (2016).
[23] F. Carreño, M. A. Antón, V. Yannopapas, and E. Paspalakis, Phys. Rev. A **94**, 013834 (2016).
[24] Y. Wu, E. D. Kim, X. Xu, J. Cheng, D. G. Steel, A. S. Bracker, D. Gammon, S. E. Economou, and L. J. Sham, Phys. Rev. Lett. **99**, 097402 (2007).
[25] A. J. Ramsay, S. J. Boyle, R. S. Kolodka, J. B. B. Oliveira, J. Skiba-Szymanska, H. Y. Liu, M. Hopkinson, A. M. Fox, and M. S. Skolnick, Phys. Rev. Lett. **100**, 197401 (2008).
[26] D. Press, T. D. Ladd, B. Zhang, and Y. Yamamoto, Nature (London) **456**, 218 (2008).
[27] D. Press, K. Greve, P. L. McMahon, T. D. Ladd, B. Friess, C. Schneider, M. Kamp, S. Höfling, A. Forchel, and Y. Yamamoto, Nat. Photon. **4**, 367 (2010).
[28] J. Hildmann and G. Burkard, Phys. Status Solidi B **251**, 1938 (2014).
[29] X. Xu, B. Sun, P. R. Berman, D. G. Steel, Allan S. Bracker, D. Gammon, and L. J. Sham, Nat. Phys. **4**, 692 (2008).
[30] D. Brunner, B. D. Gerardot, P. A. Dalgarno, G. Wüst, K. Karrai, N. G. Stoltz, P. M. Petroff, and R. J. Warburton, Science **325**, 70 (2009).
[31] K. M. Weiss, J. M. Elzerman, Y. L. Delley, J. Miguel-Sanchez, and A. Imamoğlu, Phys. Rev. Lett. **109**, 107401 (2012).
[32] J. Houel, J. H. Prechtel, A. V. Kuhlmann, D. Brunner, C. E. Kuklewicz, B. D. Gerardot, N. G. Stoltz, P. M. Petroff, and R. J. Warburton, Phys. Rev. Lett. **112**, 107401 (2014).
[33] H. S. Nguyen, G. Sallen, C. Voisin, Ph. Roussignol, C. Diederichs, and G. Cassabois, Appl. Phys. Lett. **99**, 261904 (2011).
[34] D. Heinze, D. Breddermann, A. Zrenner, and S. Schumacher, Nat. Commun. **6**, 8473 (2015).
[35] A. Delteil, Z. Sun, W.-B. Gao, E. Togan, S. Faelt, and A. Imamoğlu, Nat. Phys. **12**, 218 (2016).
[36] C. H. H. Schulte, J. Hansom, A. E. Jones, C. Matthiesen, C. Le Gall, and M. Atatüre, Nature (London) **525**, 222 (2015).
[37] W. Fang, Q.-L. Wu, S.-P. Wu, and G.-X. Li, Phys. Rev. A **93**, 053831 (2016).
[38] R. J. Warburton, C. Schäflein, D. Haft, F. Bickel, A. Lorke, K. Karrai, J. M. García, W. Schoenfeld, and P. M. Petroff, Nature **405**, 926 (2000).
[39] M. E. Ware, E. A. Stinaff, D. Gammon, M. F. Doty, A. S. Bracker, D. Gershoni, V. L. Korenev, Ş. C. Bădescu, Y. Lyanda-Geller, and T. L. Reinecke, Phys. Rev. Lett. **95**, 177403 (2005).
[40] M. O. Scully and M. S. Zubairy, *Quantum Optics* (Cambridge University Press, Cambridge, 1997).
[41] M. Lax, Phys. Rev. **172**, 350 (1968).
[42] J. P. Clemens, P. R. Rice, P. K. Rungta, and R. J. Brecha, Phys. Rev. A **62**, 033802 (2000).
[43] D. F. Walls and P. Zoller, Phys. Rev. Lett. **47**, 709 (1981).
[44] M. J. Collett, D. F. Walls, and P. Zoller, Opt. Commun. **52**, 145 (1984).
[45] L. Knoll, W. Vogel, and D. G. Welsch, J. Opt. Soc. Am. B **3**, 1315 (1986).
[46] W. Vogel and D. G. Welsch, *Lectures in Quantum Optics* (Akademie-Verlag, Berlin, 1994).
[47] H.-T. Tang, H.-X. Xia, and G.-X. Li, J. Phys. B: At. Mol. Opt. Phys. **42**, 125502 (2009).
[48] S.-Y. Gao, F.-L. Li, and S.-Y. Zhu, Phys. Rev. A **66**, 043806 (2002).